Estimation of iron contamination in Si solar cells by ideality factor: deep neural network approach

Abstract

Defect-assisted recombinations often restrict the performance of photovoltaic devices and in order to mass-produce reliable solar cells low cost express methods are in demand//required which could control/monitor contamination during the process of manufacture. In our work/research/investigation, we applied the deep learning-based approach for estimating iron concentration in silicon solar cells by 1.using numerical data on ideality factor 2. using ideality factor obtained /measured for ...(разных образцов, например??)3. by using the ideality factor of different values. The simulation of solar cells with the back surface field design for generating labeled training and test datasets was performed using SCAPS-1D software. Our results demonstrate that deep neural networks can predict iron concentration using the ideality factor, temperature, base-thickness and doping level of solar cells. Our simulation showed smaller prediction errors at high doping level, low temperature and 1. the two values of ideality factor 2. the ideality factor of 2 for structures containing only iron interstitial atoms and structures where Fe_i and iron-boron pairs coexist. The proposed method was tested on real silicon structures.

The low-cost and express methods of impurity contamination control are in demand at solar cell manufacturing. In this paper, we applied deep learning-based approach to extract the iron concentration in silicon solar cells from an ideality factor values. SCAPS-1D was the software of choice for the simulation of solar cells with the back surface field design and for the generation of labeled training and test datasets. Our results demonstrated the deep neural network ability to predict iron concentration by using ideality factor values, temperature, and base thickness as well as doping level of a solar cell. The simulation shows that the prediction error is reduced for high doping level, low temperature, and using the two values of ideality factor (for structure with interstitial iron atoms only as well as for structure with coexistence of Fe_i and iron-boron pair). The capability of functioning of the proposed method is verified for real silicon structures.

Introduction

Metal contamination control remains an important challenge for processing silicon in microelectronics, logic technologies and manufacture of solar cells (SCs) []. Typically, metal related defect characterization is performed// metal related defects are detected// metal related defects are characterised by Fourier-transform infrared spectroscopy, electron-paramagnetic resonance, minority carrier lifetime measurements, deep level transient spectroscopy (DLTS), Laplace DLTS, etc []. However, these techniques are time-consuming, require special equipment or/and specially prepared samples. At the same time, a rapid standard characterization technique mostly//widely used in industry today is current-voltage (IV) measurements. IV characteristics contain important information about electrically active defects []. Researchers propose several methods based on IV characteristics to diagnose the defects [] and consider//analize temperature dependences of current components or IV differential parameters []. These methods, however, require numerous IV measurements of high accuracy.

In our previous work [], we show that iron concentration (N_Fe) can be estimated by using SC ideality factor value (n)// ideality factor of (n), which is used quite often to characterize semiconductor barrier structures of different types []. However, the defect signatures are convoluted// are interwound (переплетаются)//intermingled (смешиваются перемешиваются) in the ideality factor with the sugnatures from many other physical processes. As a result, the obtained analytic expressions//the analytically//theoretically obtained expressions for N_Fe=f(n) are not general//universal and numerous grading curves have to be calculated/found/determined; moreover, IV must be measured over a (wide?) temperature range [].

Новый абзац Over the last decade, various fields of theoretical and applied physics have successfully been solving different problems by using deep learning methods which do not involve rigid algorithmization []. The authors claim [] that materials informatics (combination of material property calculations/measurements and algorithms of informatics) has become the fourth (along with theory, simulations and experiments) paradigm of science. In our work too we apply deep learning for predicting iron concentration from the ideality factor value (so to say "deep learning for deep levels"), but unlike in [], we applied it 1. for simulations? of the back surface field (BSF) n+-p-p+ structure and investigated the influence of the base thickness on ideality factor. //2. to the back surface field (BSF) n+-p-p+ structure and investigated the influence of the base thickness

on the ideality factor. // 3. to study the back surface field (BSF) n+-p-p+ structure and influence of the base thickness on the ideality factor.

In our previous work [], we show that the SC ideality factor value (n)// ideality factor of (n) can be used to estimate the iron concentration (N_Fe). It should be noted that the ideality factor is quite often used to characterize the various semiconductor barrier structures []. However, a defect's signature in an ideality factor is convoluted with those from so many other physical processes. As a result, obtained analytic expressions N_Fe=f(n) are not general and the numerous grading curves are required to determine; besides the IV measurements over a temperature range are necessary []. On the other hand, in the last decade, deep learning, which enables solving problems without clear algorithmization, has been successfully used in various fields of theoretical and applied physics []. Furthermore, materials informatics (combination of material property calculations/measurements and informatics algorithms) has been asserted [] to become the fourth (along with theory, simulations, and experiments) paradigm of science. This work aims to apply the deep learning approach for predicting the iron concentration from the ideality factor value (so to say "deep learning for deep levels"). Further, unlike in previous work [], the back surface field (BSF) n+-p-p+ structure was under consideration and the influence of the base thickness on ideality factor was taken into account as well.

In our work, as an approximation, we consider a rather simple system that consists of crystalline silicon (c-Si) SC and iron impurity. Despite its simplicity, the system is// can be//could be (могла бы) important for practical applications since silicon solar cells constitute ~90\% of current global production capacity [] and BSF is one of the popular designs used for industrial mass production of c-Si SCs []. Iron in these structures is the main and one of the most detrimental metallic impurities []. The flowchart of the heuristic approach we used is shown in Fig.1 where the following steps can be distinguished. First, the dark IV characteristics were simulated for SCs with known contaminant composition and various//varied (разными, которые меняли)//different (которые отличались друг от друга) parameters (если parameters относится к солнечным батареям, то переставить местами с known contaminant composition). In our numerical simulation, we applied SCAPS-1D [] widely used to model solar cells []. Second, the obtained IV curves were fitted according to the double-diode model and the ideality factors were estimated. In the result, the labeled datasets were produced. Obviously, the labeled dataset from experimental IVs would be preferable, but in practice it

is almost impossible// quite difficult to find thousands of samples with the required parameters. Third, the deep neural network (DNN) was trained to estimate iron contamination by using SC's base thickness, doping level, temperature and the ideality factor value. Fourth, the DNN was tested by using both synthetic and experimental IV curves.

As the approximation to the practical using, the paper considers a fairly simple system that consists of crystalline silicon (c-Si) SC and iron impurity. However, the system is important in practice. Silicon solar cells constitute ~90\% of current global production capacity [] and BSF is one of the popular designs used for industrial mass production of c-Si SCs []. Iron is a major as well as one of the most detrimental metallic impurities in c-Si SCs []. The flowchart of the used heuristic approach is shown in Fig.1. The following constituents can be marked out. First, the dark IV characteristics are simulated for SCs with known contaminant composition and various parameters. In our numerical simulation we applied SCAPS-1D [], which widely used to model solar cells []. Second, the obtained IV curves are fitted according to the double-diode model and the ideality factors are estimated. As a result of the aforesaid steps, the labeled datasets were produced. Obviously, the labeled dataset from experimental IVs would be preferable, but it is practically difficult to find the thousands of samples with the required parameters. Third, the training of deep neural network (DNN) to estimate iron contamination by using SC's base thickness, doping level, temperature, and ideality factor value. Fours, the DNN testing by using synthetic IV curves as well as experimental IV curves.

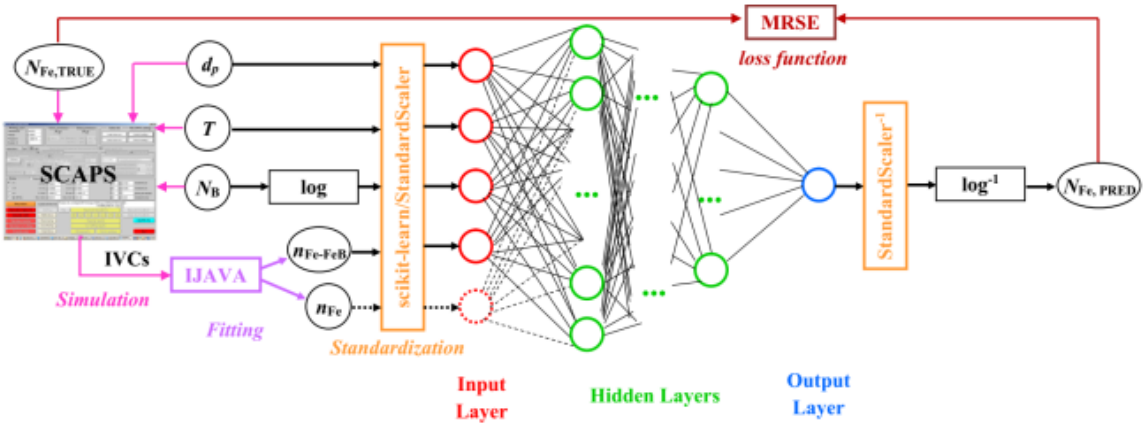

Исправлено Fig.1. Scheme of deep learning-based approach for predicting iron concentration. Additional details are discussed in the body of the article.

Simulation Details

The n+-p-p+ structure used in calculations had 0.5 μm thick emitter layer n+ with donor concentration N_D=10^19 cm-3; p and p+ were uniformly doped with boron; the base p had the thickness d_p=150-240 μm and dopant concentration N_B=10^15-10^17 cm-3; the BSF-layer p+ had the thickness d_BSF=1 μm and the acceptor concentration N_BSF=510^18 cm-3.

The simulations were carried out over the temperature range 290-340 K. For each temperature, the SCAPS setting file was created by using the following material parameters: the bandgap E_G and bandgap narrowing DeltaE_G models taken from Passler [] and Yan and Cuevas [] respectively:

(1)

where E_G0=1.1701 eV, alpha=3.2310^-4 eV/K, Theta=446 K, Delta=0.51. The carrier thermal velocities were calculated from models by Green []:

The presented calculation uses n+-p-p+ structure: the emitter layer n+ with the donor concentration N_D=10^19 cm-3 and the thickness 0.5 μm; p and p+ are uniformly doped with boron; the base p with the thickness d_p=150-240 μm is doped with concentration N_B=10^15-10^17 cm-3 and the BSF-layer p+ with the thickness d_BSF (1 μm) and the acceptor concentration N_BSF (510^18 cm-3).

The simulations were carried out over the temperature range 290-340 K. The SCAPS setting file was created for each temperature using the following material parameters. The bandgap E_G and bandgap narrowing DeltaE_G models are, respectively, from Passler [] and Yan and Cuevas []:

(1)

where E_G0=1.1701 eV, alpha=3.2310^-4 eV/K, Theta=446 K, Delta=0.51. The carrier thermal velocities were calculated from models by Green []:

(2)

изменено: where m_0 is a free electron mass. The effective state density masses in the conduction band m_dC and valence band m_dV were calculated according to models from Couderc et al. []:

(3)

The carrier mobilities and the free carrier effective masses were taken from Klaassen [] and O'Mara et al. [], respectively. The temperature and doping dependences of Auger recombination coefficients were calculated from models by Altermatt et al. []:

(4)

The band-to-band radiation recombination coefficient was taken from Nguyen et al. [].

The outside surface recombination with electron and hole velocities 10^3 cm/s were taken into account.

The simulations were carried out under the assumption that defect–assisted recombination corresponds only to iron–related deep level. As the base and the SBF-layer are uniform contaminants, iron is assumed to be in concentration N_Fe=10^10-10^13 cm-3. The simulations were performed for the following two cases. In the first case, the concentration of totally dissolved iron was given by a sum of concentrations of the interstitial iron Fe_i and trigonal iron-boron pairs Fe_iB_s:

(5)

The defect distributions are inhomogeneous, and depend on the Fermi level F position, and are given by []:

(6)

Where E_b=0.582 eV is the binding energy of FeB pairs, E_Fe is the donor level associated with Fe_i. This case corresponds to the equilibrium condition and in this article it will be referred to as ``Fe-FeB''.

In the second case, Fe_i was assumed to be homogeneously distributed (N_Fe_i=N_Fe). This condition can be realized by heat treatment (210 C, 3~min) [] or intense illumination [] and will be referred to as ``Fe''.

The donor level E_Fe_i = E_V+0.394 eV with electron sigma_n=3.47 10^-11 cm and hole sigma_p=4.5410^-16 cm capture cross-sections [] is associated with Fe_i in simulations. The donor level E_D= E_V+0.10 eV, sigma_n=410^-13 cm, sigma_p=210^-14 cm and acceptor level E_FeB= E_C-0.26 eV, sigma_n=5.1 10^-9, sigma_=3.32 cm [] are used for FeB.

The dark forward IV characteristics were generated by SCAPS over a voltage range up to 0.45 V. According to the two-diode model, the dark SC current is given by []

(7)

where I_01 and I_02 are the saturation currents, R_sh and R_s are the shunt and series resistances. The two-diode model is often used for describing real Si SCs, therefore the simulated data were fitted by Eq. (1) with n, I_01, I_02, R_sh, and R_s as fitting parameters. The fitting was performed by meta--heuristic method IJAVA []. It should be noted that the influence of both R_s (obtained values <10 Ω) and R_sh (obtained values >108 Ω) can be neglected in simulated (смоделированном)IV// in IV simulation (при моделировании IV).

In our further calculations we used the ideality factors obtained in Fe-case and Fe-FeB-case which are referred to as n_Fe and n_Fe-FeB hereafter. The typical simulated dependences of the ideality factor are shown in Fig. 2. The detailed discussion about n_Fe and n_Fe-FeB values are presented elsewhere [], however it should be noted that

(i) n can take equal values for different values of SC parameters;

(ii) dependences of n_Fe and n_Fe-FeB vary/differ (отличаются друг от друга) not only in absolute values but also in behavior, although slightly. (хотя и не сильно) insignificantly (незначительно)

Deep neural network models

изменено Deep neural network training requires a large number of samples. In order to build a training dataset, we used IV characteristics simulated by using 4 d_p values, 9 N_B values, 11 T values and 19 N_Fe values.// the values obtained for….. These values of the base thickness, doping level, temperature, and iron concentration (убрать и соединитть два предложения) which are regularly distributed (for T and d_p in linear scale, for N_Fe and N_B in logarithmic scale) over the ranges 150-240 μm, 10^15-10^17 cm, 290-340 K, and 10^10-10^13 cm, respectively. Therefore, 7524 IV characteristics were simulated in Fe-case and in Fe-FeB-case to build a training dataset (убрать?, и так понятно).

In addition, several test datasets were prepared. The d_p, N_B, and N_Fe values, which are equal to those used in training dataset, and T values, which are different, were used to build the test dataset labeled ``T-varied''. This dataset is based on 894 pairs of IV characteristics. The similar approach was used to prepare ``d-varied'' (1189 samples), ``Fe-varied'' (856 samples), and ``B-varied'' (514 samples) test datasets. The base thickness, doping level, temperature, and iron concentration values which are different from

those in training dataset values were used to prepare ``All-varied'' что?dataset?(684 samples).

Besides, several test datasets are prepared. The d_p, N_B, and N_Fe values, which equal to values from training dataset, and T values, which is divergent from training dataset, are used to build the test dataset, labeled ``T-varied''. This dataset is based on 894 pairs of IV characteristics. The similar approach was used to prepare ``d-varied'' (1189 samples), ``Fe-varied'' (856 samples), and ``B-varied'' (514 samples) test datasets. The base thickness, doping level, temperature, and iron concentration values, which are divergent from training dataset values, are used to prepare ``All-varied'' (684 samples).

The precise values of parameters are listed in Supplementary Material.

We have tried to construct a DNN that could/can estimate iron contamination by using SC parameters (d_p and N_B), measured temperatures, and the result of IV fitting (ideality factor value). As shown in Fig. 2, two DNNs with different input parameters are under consideration. The input sample of the first DNN consists of d_p, log(N_B), T and n_Fe-FeB. In practice, this input set can be obtained from one dark IV measurement. This neural network is referred to as DNN_FFB hereafter. The second DNN uses d_p, log (N_B), T, n_FFB and n_F in the input layer. In practice, to obtain a set like this additional SC processing (e.g., intense illumination) and two IV measurements are required. Further on this neural network is referred to as DNN_FFBF.

The precise values of parameters are listed in Supplementary Material.

We have tried to construct the DNN, which can estimate iron contamination by using SC parameters (d_p and N_B), measurement temperature, and the result of IV fitting (ideality factor value). As it is shown in Fig. 2 two DNNs with different input parameters were under consideration. The input sample of the first one consist of d_p, log(N_B), T, n_Fe-FeB. In practice, this input set can be obtained from one dark IV measurement. This neural network is referred to as DNN_FFB hereafter. The second one uses d_p, log (N_B), T, n_FFB, n_F in the input layer. In practice, the obtaining of such a set requires additional SC processing (e.g., intense illumination) and two IV measurements. The label DNN_FFBF is used below.

The dense deep neural network was implemented through a high-level Keras API provided by TensorFlow []. The input layers

consisted of four or five nodes -- see Fig. 1. In the output layer, one node and linear activation were used. The five configurations of the hidden layers were under consideration// analized//considered:

(i) ``pipe'': each hidden layer contains equal number of nodes;

(ii) ``trapezium'': six hidden layers, number of neurons linearly decreases from 100% (the first layer) to 50% (the last layer);

(iii) ``triangle'': ten layers, the number of neurons linearly decreases from 100% (first layer) to 10% (last layer);

(iv) ``butterfly'': two serial reflected trapezium configurations;

(v) ``fir'': two serial trapezium configurations.

The dense deep neural network was implemented through the high-level Keras API provided by TensorFlow []. The input layers consist of 4 or 5 nodes -- see Fig. 1. 1 node and linear activation were used in the output layer. The five configurations oh hidden layers were under consideration:

(i) ``pipe'': each hidden layer contains equal number of nodes;

(ii) ``trapezium'': six hidden layers, number of neurons linearly decreases from 100% (first layer) to 50% (last layer);

(iii) ``triangle'': ten layers, number of neurons linearly decreases from 100% (first layer) to 10% (last layer);

(iv) ``butterfly'': two serial reflected trapezium configurations;

(v) ``fir'': two serial trapezium configurations.

The mean squared relative error (MSRE) was chosen as the loss function:

(5)

where N_s is the number of samples in the dataset, N_TRUE is the iron concentration used in the i-th sample simulation and N_PRED is the DNN prediction for the i-th sample.

Hyperparameters include the number of nodes for the first hidden layer, the number of hidden layers (in pipe configuration), batch size, activation function, optimizer, learning rate, preprocessing method, dropout rate, regularization function,regularization rate and weight initializer. A grid search (coarse tuning to limit one hyperparameter)

and random search (fine tuning) were performed over the predefined space, shown in Table 1, and the best hyperparameter combination was chosen.

The mean squared relative error (MSRE) was chosen as the loss function:

(5)

where N_s is the number of samples in dataset, N_TRUE is the iron concentration, which was used in simulation of i-th sample, N_PRED is the DNN prediction for i-th sample.

Hyperparameters include the number of nodes for the first hidden layer, the number of hidden layers (in pipe configuration), the batch size, the activation function, the optimizer, the learning rate, the preprocessing method, the dropout rate, the regularization function, the regularization rate, and the weight initializer. A grid search (coarse tuning to limit one hyperparameter) and random search (fine tuning) were performed over the predefined hyperparameter space, shown in Table 1, and the best hyperparameter combination is chosen.

To estimate DNN training, 10--fold cross--validation was used. The performance of the DNN models on test datasets was evaluated by using three metrics: MSRE coefficient of determination R^2 and coefficient of correlation R. Finally, to increase a DNNs performance, a full dataset consisting of training dataset and all the test datasets was used for the training models (для обучающих моделей?).

10--fold cross--validation was used to estimate DNN training. The MSRE, coefficient of determination R^2, and coefficient of correlation R were three metrics used to evaluate the performance of the DNN models on test datasets. Finally, to increase a DNNs performance, the full dataset, which consists of training dataset and all test datasets, was used for the training models.

Results and Discussion

Synthetic IV curves

The results of hyperparameter search are listed in Table 2. In particular?? (зокрема? тогда вторая конструкция лучше), 1. the trapezium and pipe configurations are chosen for DNN_FFB and DNN_FFBF respectively. 2. for DNN_FFB and DNN_FFBF the trapezium and pipe configurations are/were? (прошлое время если

выбор был сделан для поиска hyperparameter) chosen, respectively.

The training and test results of DNN_FFB are presented in Table 1, Table 2, and Fig. 3. As seen, MSRE of DNN_FFB prediction is sufficiently large. However, it should be noted that 1. in most cases the fraction//part??//number of predictions?? is not great // 2. in most cases the predictions with big differences between N_TRUE and N_PRED are not numerous. In particular, squared relative error (SRE) does not exceed 0.05 for 87%, 88% and 96% for samples from T-varied, d-varied and Fe-varid datasets respectively --- see bars in Fig. 1. In the B-varied dataset (1. with doping level value non--used in the training dataset (in the training dataset если относится к B-varied datase, то убрать)// 2. without doping level value), the biggest MSRE=1.06 is associated with those not often samples that have a really great SRE (>20) while SRE is less than 0.05 in 54% for samples from the B-varied test dataset (не понимаю зачем это нужно повторять)?. The worst predictions are quite expectedly to be observed for the All-varied dataset: R^2 equals 0.813 and SRE is only 0.05 for 18% smaller (тоже непонятно). On the other hand, the Fe-varied dataset is most similar to real demand?. In this case (тоже не понятно какой случай имеется в виду) the determination and correlation coefficients are high enough (0.991 and 0.996).

Results and Discussion

Synthetic IV curves

The results of the hyperparameter search are listed in Table 2. In particular, the trapezium and pipe configurations are chosen for DNN_FFB and DNN_FFBF respectively.

The training and test results of DNN_FFB are presented in Table 1, Table 2, and Fig. 3. As we can see, that MSRE of DNN_FFB prediction is sufficiently large. But it should be noted that the fraction of prediction with a big difference between N_TRUE and N_PRED is not numerous in most cases. Thus squared relative error (SRE) does not exceed 0.05 for 87%, 88%, and 96% samples from T-varied, d-varied and Fe-varid datasets respectively --- see bars in Fig. 1. For the B-varied dataset (with doping level value, non--used in the training dataset) the biggest MSRE=1.06 connects to the occurrence of some samples with a really big SRE (>20). While SRE is less than 0.05 in 54% of samples from the B-varied test dataset. The worst predictions are quite expectedly to be observed for the

All-varied dataset: R^2 equals 0.813 and SRE is less than 0.05 for 18% only. On the other hand, the Fe-varied dataset is most similar to real demand. And determination and correlation coefficients are high enough (0.991 and 0.996) in this case.

We have also considered/ analyzed the DNN prediction error versus SC parameters --- see Figs.1-3. The figures present data for training dataset; the results for test datasets are similar. In particular, Fig. 1(a) shows a considerable increase in prediction error, which is observed at T>320 K for DNN_FFB. As seen from (Fig. 2(c), at T=340 K the maximum SRE is about 20 and SRE below 0.01 is observed for 55% of the samples whereas SRE of 0.02 is for 83% at T=290 K (Fig. 3(b). It has been shown previously [] that temperature rise causes the increase in the intrinsic recombination contributions to the ideality factor. As a result, the sign of Shockley-Read-Hall (SRH) recombination in n value becomes less evident//prominent//prnounced and DNN predictive ability decreases.

The dependencies on DNN prediction error on SC parameters values are under consideration too --- see Figs.1-3. These figures represent data for the training dataset, the results for test datasets are similar. Thus Fig. 1(a) shows that the considerable increase in prediction error value is observed at T>320 K for DNN_FFB. So the maximum SRE is about 20 and the SRE is less than 0.01 for 55% of samples at T=340 K (Fig. 2(c)). Whereas those values are equal to 0.02 and 83% at T=290 K (Fig. 3(b)). It has been shown previously [], that temperature rise causes the increase in the intrinsic recombination's contribution to an ideality factor. As a result, the sign of Shockley-Read-Hall (SRH) recombination in n value become less evident and DNN predictive ability falls.

As shown in Fig. 4, the SC base thickness practically (почти??) does not influence the prediction error (the mean value as well as relative frequency). However, as seen from Fig 5(c,d), the ideality factor value (лучше убрать, если и так понятно) depends on base thickness at constant N_Fe. Therefore d_p is a significant parameter for DNN training.

The predictive error increases sharply as the doping level decreases --- see Fig. 2(a). In particular, the maximum SRE is about 0.05 for N_B=10^17 cm (Fig. 3(c)) whereas below 0.05 SRE is for 56% of the samples only for //with N_B=10^15 cm (Fig. 3(b)). The occupation of holes in Fe-related level determines SRH recombination efficiency. According to the Fermi-Dirac statistics, the probability of hole

occupation in a non-degenerate p-type semiconductor with full acceptor depletion can be expressed as

(6)

If N_B decreases, the level is filled with electron, the SRH recombination is accomplished and the ideality factor value sharply decreases --- Fig. 5(a,b). Moreover, in case of low doping, impurities have only a weak influence on the ideality factor and therefore the increase of MSRE is observed. And finally, we believe that an additional factor causing the error increase at high temperatures is the level filling.

The predictive error rises sharply with doping level decrees --- see Fig. 2(a). Thus maximum SRE is about 0.05 for N_B=10^17 cm (Fig. 3(c)) whereas squared relative error is less than 0.05 for 56% of samples only for N_B=10^15 cm (Fig. 3(b)). The hole occupation of the Fe-related level determines the SRH recombination efficiency. Accordingly to the Fermi-Dirac statistics, the probability of a hole occupation in a non-degenerate p-type semiconductor with full acceptor depletion can be expressed as

(6)

If N_B decreases, the level is filled with an electron, the SRH recombination ceases, and the ideality factor value sharply reduces --- Fig. 5(a,b). Besides, a weak influence of impurities on ideality factor under low doping conditions is a reason for observed MSRE increase. In our opinion, the level filling is an additional reason for an error increase at high temperatures as well.

Fig. 6(a) shows that MSRE increases at both low and high iron concentrations. The first N_Fe area of poor DNN accuracy is entirely predictable, the second one seems to be rather surprising. But according to Fig 4(c), the MSRE increase is most likely to be due to the fact that only a few samples have// are predicted with a great SRE whereas SRE increases more systematically when N_{Fe}=10^13 cm --- Fig 5(b).

The ideality factor value for the case when only interstitial iron (n_Fe) is available gives additional information about the defects in comparison with n_FF}. It is not surprising that DNN_FFBF has better operating parameters in comparison with DNN_FFB --- see Table 3, Table 4 and Fig. 5. The operation improves at the decreased MSRE when there is no huge (огромной - не слишком ли сильно сказано) difference between the values of N_TRUE and N_PRED} and the

range of SRE is narrow (Figs. 3-6). As shown in Fig.4, the maximum SRE does not exceed one even in the case of All-varied datasets and SRE is below 02 for 93%, 92%, 73% and 97% of the samples of//in/for T-varied, d-varied, B-varied, and Fe-varied datasets respectively. It should be noted that for Fe-varied datasets both R^2 and R are (0.999).

Fig. 6(a) shows that MSRE increases at both low and high iron concentrations. The first N_Fe area of bad DNN accuracy is entirely foreseeable, the second one is surprising enough. But accordingly to Fig 4(c), the MSRE increasing at N_Fe=10^13 cm is most likely determined by a few samples with big SRE value. Whereas SRE increasing is more systematic at N_{Fe}=10^13 cm --- Fig 5(b).

The ideality factor value for the case of interstitial iron only presence (n_Fe) gives additional information about defects in comparing with n_FF}. It is not surprising that DNN_FFBF has better operating parameters in comparing with DNN_FFB --- see Table 3, Table 4, Fig. 5. The operation improvement appearances in the MSRE decrease as well as in absence of huge difference between N_TRUE and N_PRED} values and narrowing of SRE range (Figs. 3-6). Really, it is shown in Fig.4 that the maximum SRE does not exceed one even in the case of All-varied datasets and SRE is less than 0.02 for 93%, 92%, 73%, and 97% of samples of T-varied, d-varied, B-varied, and Fe-varied datasets respectively. The R^2 (0.999) and R (0.999) values for Fe-varied dataset draws attention as well.

Despite the difference in prediction accuracy, the features of DNN_FFBF and DNN_FFB are similar. Thus, the DNN training with N_B values, which is expected to be an object of future research, is important for prediction accuracy (Fig. 2); the increase in the temperature (Fig. 3) as well as decrease in doping level (Fig. 5) or iron concentration (Fig. 6) results in error increse. It should be noted that the prediction error gain with N_Fe increase is not observed in case of DNN_FFBF and the range of SRE at N_Fe=10^13 cm is narrower than at N_Fe=10^10 cm --- see Fig.8(b,c).

Despite the difference in predicting accuracy, DNN_FFBF features are similar to DNN_FFB ones. Thus the DNN training with N_B values, which are expected in object of future research, is important for prediction accuracy (Fig. 2); the increase in the temperature value (Fig. 3) as well as decrease in doping level (Fig. 5) or iron concentration (Fig. 6) results in error rise. It should be noted that the prediction error gain with N_Fe increase not observed in DNN_FFBF case and SRE range at N_Fe=10^13 cm is more narrow then those at N_Fe=10^10 cm --- see Fig.8(b,c).

The results of both DNN_FFB and DNN_FFBF training with a full dataset are presented in Table 3, Fig.6(f) and Fig.7(f).We can see that in our case the extension of the labeled dataset practically does not improve the result of DNN. In our opinion, there is evidence of// this is evidence of?? of

i) good DNN configuration tuning;

ii) restricted predictive ability of DNN_FFB, which is caused by ambiguity of dependence n_FFB=f(N_Fe).

The results of training both DNN_FFB and DNN_FFBF with full dataset are presented in Table 3, Fig.6(f), and Fig.7(f). One can see that the extension of the labeled dataset does not practically improve the DNN result in our case. In our opinion, there is evidence of

i) a good DNN configuration tuning;

ii) a limited predictive ability of DNN_FFB, which caused by ambiguity of dependence n_FFB=f(N_Fe).

Experimental IV curves

The ability of DNNs to predict iron concentration in real silicon SCs was tested as well. The samples used in the experiment were n+-p-p+--Si structured. The structures were fabricated (имеется в виду промышленное изготовление?)//prepared/produced from p-type boron doped Czochralski silicon wafer with [100] orientation and resistivity of 10 Ohm (N_B = 1.410^15 cm). The n+ emitter with surface resistance of about (20-30) Ω and thickness of 0.7 μm was formed by phosphorus diffusion at 940C. 1. p+ layer ((10-20) Ω, 0.6 μm) formed by boron diffusion at 985C served as an anti-recombination isotype barrier. 2. As the anti-recombination isotype barrier we used p+ layer ((10-20) Ω, 0.6 μm) formed by boron diffusion at 985C. The base thickness was 350 μm and the area of the samples was 1.52χ1.535 cm . The concentration of iron in the SC base N_MEAS was determined from kinetics of the short circuit current under monochromatic illumination []. Two samples used in the investigation are referred to as SC320 and SC349 with N_MEAS of (2.0-0.4)10^12 cm and (6.7-0.7)10^12 cm, respectively.

The ability of DNNs to predict the iron concentration in real silicon SCs was tested as well. The n+-p-p+--Si samples were used in the experiment. The

structures were fabricated from p-type boron doped Czochralski silicon wafer with [100] orientation and a resistivity of 10 Ohm (N_B = 1.410^15 cm). The n+ emitter with a surface resistance of about (20-30) Ω and a thickness of 0.7 μm was formed by phosphorus diffusion at 940C. The anti-recombination isotype barrier was created by using p+ layer ((10-20) Ω, 0.6 μm), which was formed by boron diffusion at 985C. The base thickness was equal to 350 μm. The samples used in the experiment had the area of 1.52χ1.535 cm. The concentration of iron in the SC base N_MEAS was determined from kinetic of the short circuit current under monochromatic illumination []. Two samples, referred to as SC320 and SC349 with N_MEAS values of (2.0-0.4)10^12 cm and (6.7-0.7)10^12 cm, respectively, were used in the investigation.

> We can see that DNN was faced with a rather difficult task when the complexity was associated with a certain mismatch between the parameters of real structures and those used in the simulation. However, the need for? iron-related defects, which predominantly determine recombination, was the main criterion for sampling in our case.

One can see that DNN was faced with a rather difficult task, in which complexity is associated with a certain mismatch between the parameters of real structures and those used in the simulation. However, the need for iron-related defects, which predominantly determine recombination, was the main criterion for sampling in our case.

> The dark I-V characteristics of the samples were measured at temperatures 300, 320, and 340 K. The measurements were carried out after 48 h exposition in the dark at room temperature (``Fe-FeB'' case) as well as immediately after intense illumination of the sample with a halogen lamp (``Fe'' case). To fit the experimental data and determine fitting parameters, in particular n, R_s, R_sh, we used Eq.(3). The typical results of the measurements and approximations are shown in Fig. 3 and Table 3. It should be noted that for real I-V curves, in contrast to synthetic ones, the influence of series and shunt resistances cannot be neglected (the magnitude of R_s is about 3 and 6 Ohm for samples SC320 and SC349, respectively, all?? the values // these values?? of Rsh are listed in Table 6).

The dark I-V characteristics of these samples were measured at temperatures of 300, 320, and 340 K. The measurements were taken after 48 h sample storage in the dark at room temperature (``Fe-FeB'' case) as well as immediately after sample intense illumination with a halogen lamp (``Fe'' case). After that, we used Eq.(3) to fit the experimental data and determine fitting parameters, in particular n, R_s, R_sh. The typical results

of measurements and approximations are shown in Fig. 3 and Table 3. It should be noted that for real I-V curves, in contrast to synthetic ones, the influence of series and shunt resistances cannot be neglected (the R_s values are about 3 and 6 Ohm for samples SC320 and SC349, respectively, the Rsh values are listed in Table 6).

> The values of the ideality factor// the ideality factor factors determined from the experimental curves and the sample parameters were used as input data for DNN_FFB and DNN_FFBF, which were trained either on training dataset or full dataset.
>
> The predictions are listed in Table 9.
>
> First of all, it should be noted that even though we did not use// consider// analyze a simulation model of extremely high complexity, the results exceeded our expectations. In particular, the predicted iron concentrations in DNN_FFB differed only several times from the measured ones. In the case of sample SC320 and DNN_FFB trained on the full dataset, the error did not exceed 40%.

The values of the ideality factor, determined from the experimental curves, and the sample parameters were used as input data for DNN_FFB and DNN_FFBF, which were trained on the training dataset or the full dataset.

The predictions are listed in Table 9.

First of all, considering the not extreme high complexity of the simulation model, we note that the results even exceed expectations. Particularly for DNN_FFB, where the predicted iron concentrations differ by only several times from the measured ones. And in the case of sample SC320 and DNN_FFB, trained on the full dataset, the error does not exceed 40%.

> Also, it should be noted that the results confirm the trends revealed by the analysis of synthetic I-V curves. In particular, the prediction accuracy decreases at T>320 K and iron concentrations close to the upper limit in the range (10^13 cm). These facts completely coincide with the data in Fig. 4a and Fig.5a, respectively. In addition, the sample's base doping level (N_B=1.410^15 cm) is not used in the training dataset but can be found in the d--varied dataset (see Supplementary Material). Table 4 shows that the prediction of DNN_FFB trained by a full database is better than in the case of learning only by a training dataset, especially for SC320 sample. This fact confirms the conclusion made in the previous section about the importance of DNN training with N_B values, which are expected to be the object of future research.

Also, it should be noted that the results confirm the trends identified during analyzing synthetic I-V curves. Namely, the prediction accuracy decreases for T>320 K and iron concentrations, which are close to the upper limit of the considered range (10^13 cm). These facts fully coincide with the data in Fig. 4a and Fig.5a, respectively. In addition, the sample's base doping level (N_B=1.410^15 cm) is not used in the training dataset but can be found in the d--varied dataset (see Supplementary Material). Table 4 shows that the prediction of DNN_FFB, trained by full dataset, is better than in the case of learning by training dataset only, especially for the SC320. This feature confirms the conclusion from the previous section about the importance of DNN training with N_B values, which are expected in the object of future research.

> On the other hand, contrary to our expectations, DNN_FFBF demonstrates worse performance than DNN_FFB in the majority case because of several reasons. First, 1. the use of two ideality factor values makes the influence of simulation simplifications more significant (e.g., the effect of unaccounted processes that cause both shunt and series resistance). 2. a simplified simulation with the use of only two ideality factors involves, for example, both shunt and series resistance which arise due to the processes that are not taken into account. Secondly, to determine// estimate/find/calculate/obtain a correct n_Fe is a more complicated experimental task than to identify n_FF. For example, in our experiment it took about 100 s to obtain I-V characteristics after intense illumination. This interval included the time required to set the temperature after illumination-induced heating and the time of measurement. According to [], the characteristic association time of FeB pairs at T=340 K and N_B=1.410^15 cm is about 600 s. Therefore, it cannot be expected that this value of the ideality factor corresponds to the complete dissociation of FeB pairs. That is, despite the potentially higher accuracy of the DNN_FFBF predictions (shown in the previous section), the practical application of this approach is more complicated.
>
> On the whole, the results obtained for real SCs confirm the possibility to estimate iron contamination using ideality factor value.

On the other hand, contrary to expectations, the DNN_FFBF demonstrate worse performance than DNN_FFB in the case majority. There can be several reasons. Firstly, the use of two ideality factor values enhances the influence of simulation simplifications (e.g., the effect of unaccounted processes that cause the appearance of both shunt and series resistance). Secondly, the correct n_Fe determination is a more complicated experimental task than n_FF identifying. For example, it took about 100 s to

obtain the I-V characteristics after intense illumination in our case. This interval consisted of time to set the temperature after illumination-induced heating as well as time to measurement. According to [], the characteristic association time of FeB pairs at T=340 K and N_B=1.410^15 cm is about 600 s. Therefore, it cannot be expected that such a value of the ideality factor corresponds to the complete dissociation of FeB pairs. That is, despite the potentially higher accuracy of the DNN_FFBF predictions (shown in the previous section), the practical application of this approach is more complex.

Generally, the results obtained for real SCs confirm the possibility of estimation for iron contamination by ideality factor value.

Conclusion and Outlook

In this paper// In our simulations, we determined iron concentration in silicon BSF solar cells from the ideality factor value and systematically studied the performance of deep learning in solving?? this problem. Our work is//It was the first attempt to use deep learning for retrieval of deep level parameters from the current--voltage curve. In the model study, we used//performed simulation in order to obtain training datasets and test labeled datasets?// training and (labeled) test datasets. In the end, DNN was trial-tested by using the parameters of actual solar cells. Our results showed the DNN ability of the deep neural network (тогда лишнее) to predict iron concentration by using ideality factor values, the thickness and doping level of SC base as well as temperature. For synthetic datasets the MSRE was to // as small as (составляла всего лишь)// comprised (составляла)// reached (достигала) 0.005. Our simulation shows the prospects for applying the ideality factor of two values (for structure with Fe_i only as well as with FeB and Fe_i coexistence) in order to upgrade prediction accuracy. At the same time, the practical application of this approach demonstrated difficulties in obtaining correct data. It was important to train the DNN with a boron concentration value// values (мне кажется так лучше и тогда без артикля), which agreed with the doping level of the structures under study. Moreover, the increase in iron or boron concentration, as well as temperature decrease, resulted in a smaller prediction error//smaller prediction errors.

In this paper, we extracted the iron concentration in silicon BSF solar cells from an ideality factor value and systematically studied the performance of

deep learning in this problem. This work is the first attempt at using deep learning for deep levels parameter retrieval from the current--voltage curve. In this model study, we used simulation to obtain training and test labeled datasets. Besides, a DNN was trial-tested by using the parameters of actual solar cells. Our results showed the ability of the deep neural network to predict iron concentration by using ideality factor values, SC base thickness and doping level, and temperature. MSRE was up to 0.005 for synthetic datasets. The simulation has shown the prospects for the use of two ideality factor values (for structure with Fe_i only as well as with FeB and Fe_i coexistence) for upgrading a prediction accuracy. At the same time, the practical application of such an approach manifested difficulties in obtaining correct data. It was important to train DNN with a boron concentration value, which agreed with the doping level of investigated structures. Moreover, the increase in iron concentration or boron concentration, as well as temperature decrease, results in a prediction error reduction.

> The proposed DNN approach uses a simple and widely applied (применяемый) setup and does not take much time. Therefore, it could be easily integrated into the manufacturing environment. It should be noted, however, that for our purposes the task was simplified. Nevertheless, we believe that this DNN approach can be further improved in two ways.The first is to refine labeled datasets by using 3D-simulators (e.g., SILVACO TCAD) or real IV measurements in a broad set of SCs. The second is to improve DNN operation, and fine-tuning seems to be most promising in this case. For example, innumerous input parameters can be multiplied and transformed into a picture so that the vision model (e.g., VGG16) could be applied.

The proposed approach envisages the utilization of a simple and widely applicable setup and does not require much time. Therefore it could be integrated into a manufacturing environment. However, it should be noted that we have simplified the task for our purposes. In our opinion, there are two ways of further improve the method. The first one connects with the refining of labeled datasets and can be realized by using 3D-simulators (e.g., SILVACO TCAD) or real IV measurements in a broad set of SCs. The improvement of DNN operation is the second one; and the fine-tuning is like most promising in this case. For example, not numerous input parameters can be multiplied and transformed to the picture and apply a vision model (e.g., VGG16).